Co-optimization of a high temperature thermal storage as per its modeling accuracy

Ibrahim Al Asmi, Roman Le Goff Latimier, Yasmine Lalau, Thomas Brian, H. Ben Ahmed

Research papers

Co-optimization of a high temperature thermal storage as per its modeling accuracy

Ibrahim Al Asmi [a,b,*], Roman Le Goff Latimier [a], Yasmine Lalau [c], Thomas Brian [b], Hamid Ben Ahmed [a]

[a] SATIE Laboratory (CNRS) - Ecole Normale Superieure of Rennes, Bruz, France
[b] R&D department Eco-Tech CERAM, Perpignan, France
[c] Université de Toulouse, IMT Mines Albi, UMR CNRS 5302, Centre RAPSODEE, Campus Jarlard, 81013, Albi, cedex 09, France

A B S T R A C T

Coupling energy networks becomes unavoidable in order to decarbonize human usages, increase global energy efficiency and ensure flexibility in so-called "multi-energy" network. In such a network, high temperature thermal energy storage (HTTES) can be a relevant solution when designed and managed in an optimal way. However, the precise modeling of its physical behavior requires complex models whose computational costs are not compatible with optimal control. A fortiori, a co-optimization approach requires to select a less precise but faster model. This article proposes to study the consequences of using a panel of such lighter models, in particular by discussing the modeling of losses. To do so, two business models will be discussed on a case study composed of a heat network linking a concentrated solar power (CSP) to thermal industrial load. When losses are not a consideration, the use of very simplistic models is sufficient to determine a good estimate of storage sizing. However, if losses are included, a proper co-optimization can only be achieved by using a metamodeling approach.

1. Introduction

In 2018, 76% of global greenhouse gas emissions (GHG) are emitted in the energy sector, where 42% of this energy is designed to meet heat and electricity needs in residential, service and industrial sectors [1]. To overcome this problem, governments and industries seek energy strategies and technical solutions to reduce the carbon footprint of the produced energy. In Europe, 78% of electricity, in the residential sector, has been consumed for space and water heating in 2020 [2]. However, considering the coupling between heat and electricity sectors is unusual today when building networks, even though it is necessary to reach a global optimal design and management. This approach is complex, as it uses innovative technologies and requires fine optimization to reach a profitable solutions, compared to standard approaches [3]. The efforts made to overcome the difficulties of a multi-energy network are justified by the numerous resources and technologies that could then be exploited much more widely than today [4]. For instance, 8900 TWh/year of waste heat can be exploited if considered when designing energy networks [5]. Moreover, the share of renewable energy in the final consumption needs to be doubled by 2030, to be on track with the net zero emissions by 2050 Scenario [1]. Hence, flexible networks will be required to accommodate important amount of intermittent energy and to meet heat and electrical needs. To achieve this, conversion systems (Power-To-Heat, Heat-To-Power...) to couple networks and multiple storage technologies do exist such as Electrochemical Energy Storage (EES) and Thermal Energy Storage (TES). TES can have many uses such as storing excess of heat or even electricity, after being converted into heat by the help of Power-To-Heat (PTH) system, during production peak periods. In the other way, TES can deliver heat or electricity, coupled to a steam turbine or an Organic Rankine Cycle (ORC), during load peak periods [6].

TES technologies are multiple and can be categorized based on their temperature, physical principle, geometry, storage medium (HSM) and heat transfer fluid (HTF) as discussed in [7]. Here, a sensible thermocline high temperature thermal energy storage (HTTES), using air as HTF and rocks as HSM, will be studied [8]. This technology has proven to be cost effective and recently undergone numerous developments as shown in [9–11]. In a multi-energy network, the HTTES system represents an important flexibility to accommodate intermittent energy resources but also to meet uncontrolled demand. The investment cost of such a system (CAPEX) can be a barrier if not optimized. In other words, if operation costs (OPEX) and benefices do not payback the CAPEX

* Corresponding author at: SATIE Laboratory (CNRS) - Ecole Normale Superieure of Rennes, Bruz, France.
E-mail address: Ibrahim.alasmi@ens-rennes.fr (I. Al Asmi).

Nomenclature

Acronyms

1D/2D	One dimension, two dimensions
BM	Business model
CED	Cumulative energy demand
CSP	Concentrated solar power
DNI	Direct normal irradiation
EPBT	Energy payback time
HT	High temperature
HSM	Heat storage material
HTF	Heat transfer fluid
LF	Logistic function
MM	Metamodel
MPC	Model predictive control
n°	Number
NRMSD	Normalized root mean square deviation
PDE	Partial differential equations
SLSQP	Sequential least squares programming
TES	Thermal energy storage

Greek Symbols

ρ	Density, (kg m^{-3})
Δ	Difference
η	Efficiency, (%)
ε	Void fraction

Latin Symbols

A	Surface area, (m^2)
C	Optimization costs, (MWh)
c_p	Heat capacity, (J K^{-1} kg^{-1})
D	Diameter, (mm)
E	Energy, (MWh)
h	Heat transfer coefficient, (W K^{-1} m^{-2})
k	Thermal conductivity, (W K^{-1} m^{-1})
L	Storage length, (m)
m	Mass, (kg)
$\dot{m}$	Mass flow rate, (kg s^{-1})
N	Time horizon, (h)
N^{years}	Operating period length, (years)
n_w	Optimization sliding window size, (h)
P	Power, (MW)
s	Thermocline slope at inflection point
S	Section, (m^2)
T	Temperature, (°C)
t	Time, (s)
u	Fluid velocity, (ms^{-1})
V	Volume, (m^3)
X	Metamodel state vector
x	Axial position, (m)
z	Thermocline position (m)

Subscripts

bed	Storage bed
blo	Reflected sunlight blocked by adjacent heliostats
cons	Simulations for model construction
c	Central
CH	Charging phase
DC	Discharging phase
design	Design cost
eff	Effective
exp	Experimental
ext	External
f	Fluid
fuel	Gas consumption
fuel-saved	Saving in gas consumption thanks to storage
fuel-saved_{max}	Saving in gas consumption with maximum investigated storage size
hel	Heliostat field
load	Load consumption
loss	Losses
loss-ch	Losses during the charging phase
mean	Mean
max	Maximum
min	Minimum
m	Measurement
mis	Difference between production and consumption
operating	Operating cost
opt	Optimization
p	Particle
prod	Production source
rated	Maximum storage rate
ref	Heliostat reflectivity
s	Solid
sto	Storage
sim	Simulation iteration
sh	Heliostat surface shaded by adjacent heliostats
shed	Over production shedding
spil	Reflected sunlight missing the receiver due to other technological errors
th	Thermal carrier
tot	Total
tra	Atmospheric transmission between the heliostat and the receiver
v	Interstitial between fluid and solid
w	Wall

over its lifetime, the system is considered as not profitable. Therefore, it is essential to co-optimize such a system coupling its design and its management to find the best compromise between both. This requires the storage to be designed and operated optimally with the help of a predictive controller that calculates the installed capacity and the management strategy. To do so, it is decisive to have a controller model enabling the anticipation of future events that would lead to a realistic optimal design and management. Additionally, within the control optimization, the chosen model requires accuracy and speed to reach the best performance within acceptable time cost adapted for real-time management applications. Moreover, the controller model needs to be suitable for the objective function that changes from case to another. Typically, a simple objective function would not consider losses of storage system. On the other hand, objective function in multi-energy network needs to consider storage losses and other terms that depends on local storage information. As a result, HTTES co-optimization requires appropriate models in terms of computation time,

accuracy but also the ability to estimate all objective function terms. Therefore, the sensitivity of HTTES co-optimization to different modeling levels need to be evaluated for different objective functions more or less complex.

1.1. State of the art

HTTES modeling have been the subject of many research and development work, mainly in the recent years. Here we will focus on time-dependent HTTES models as they allow the anticipation of future events based on the current state of the system. Most of those models solve partial differential equations (PDE) to estimate precisely the evolution of the system temperature respecting the energy conservation principle. Those models are relatively time consuming but relevant for simulation purposes along several cycles. [12–14] describe some of commonly used models in the literature, that solve PDE along one or two spacial dimensions (1D and 2D). It is to be noticed that in 1D models, radial effects are neglected compared to 2D models. [15] investigated three hot water TES models of increasing complexity level. They stated that accurate modeling of losses and storage temperature has an impact on the profitability of the projects. [16] proposes and experimentally validates 1D models based on PDE by the help of an oil/rock HTTES prototype. A similar model for air/rock HTTES has been conducted by [17], where radial effects have been neglected to achieve 1D model. Besides, other work focused on developing models without solving PDE to avoid computation time limitation. [18] describes a model based on an analytical formulation, used to calculate the storage temperature evolution with low computation time but only for partial cycle configurations. [19] proposed a new algebraic formulation of the developed model in [20,21]. In this formulation, the algebraic solution for thermocline HTTES is given as polynomial function, and allowing for any initial temperature profile to predict the storage temperature evolution. [8] suggested a metamodel based on data issued from 1D - PDE model simulations, representing a suitable trade-off between accuracy and computation time. In case of manufacturing defects or highly dimension-dependent phenomena like flow channeling, this metamodel can be constructed on data issued from experimental measures. However, researchers conclude that such an experiments based metamodel requires experimental validation.

The state of the art shows that, thermal storage optimization research are mainly conducted to calculate the optimal design or the management strategy. 0D models are often used for those purposes as they have low computation time adapted for predictive controller usages. Model Predictive Control (MPC) has been developed, to define the optimal thermal storage strategy for a heat network case study, in [22–24]. Other studies such as [25] investigate the operational optimization of a heat district network using TES and solving Mixed Integer Linear Programming (MILP) problem. Researchers agree that 0D models can by used for a quick estimation of large systems optimal design and management. It is to be mentioned that, in all those studies, simulation and optimization models are identical. Moreover, [26,27] study the design optimization, whereas [28] investigates the pricing and the management, of a multi-energy system at the scale of a region. The models involved in these works are 0D in order to guarantee reasonable computation time and low complexity level. The impact of coupling management and design when optimizing a storage system had been a subject of interest of several papers in EES field. [29] studied the impact of forecasting models on the sizing of electrical vehicle fleet, where batteries are charged by the help of a photovoltaic power plant. It appeared that the forecast model quality impact the optimal battery size but author recommend further investigations. [30] investigated the impact of battery aging model on the management and design results. Researchers conclude that introducing an aging model, even a simplistic one, greatly improves the choice of storage capacity. Three EES models of different accuracy level, used for optimal design, have been explained in [31]. It concludes that a temperature model is necessary when it impacts the controller actions. In addition, introducing aging into controller models can have important impact on the rate of degradation. Researchers conclude that trade-offs between model complexity and model accuracy can be difficult to navigate, but offer significant benefits in terms of performance.

This review shows that multiple models of HTTES exist with increasing level of complexity and accuracy. However, most of optimization work related to HTTES uses 0D models for computation time reasons. On the other hand, a 1D metamodel based on experience was proposed but lack experimental validation. Moreover, the state of the art shows that the impact of the model choice on the HTTES management and design was not evaluated. Also, most of works study either the management or the design of the HTTES but, to our knowledge, none of them study the co-optimization of this system.

1.2. Scope of this work

The goal of the present contribution is to study the impact of the HTTES model choice on the performance of the simulator and the co-optimization controller for two case studies. Therefore, four models of increasing complexity, including models that consider losses and others that does not, are being selected from the literature and investigated. Also, the first case study is formulated with simple objective function that does not take into account losses. On the contrary, the second case study takes into account losses in the objective function. The impact of model choice is measured by the help of time, management and design cost. For this purpose, a new physical metric is formulated to evaluate management and design costs. As a result, suitable trade-off between accuracy and computation time can be found for future real-time management and design purpose. Also, the impact of model choice, in function of its accuracy and computation time, on the co-optimization results is being analyzed for different storage capacities. Moreover, 1D metamodel based on measured data is being studied in the case of HTTES with manufacturing defects. This metamodel is constructed on the bases of four experiments and being validated over three days of continuous experimental tests by the help of an HTTES test facility in the south of France.

Section 2 presents the selected models from the literature that are used along this article. Section 3 describes the case study used to conduct the co-optimization study, the mathematical formulation as well as the optimization algorithm. Section 4 discuss simulations models and evaluate their performance. Also, in case of defected installation, metamodel based on experimental measures is discussed as well as the facility, experimental protocol and instrumentation used for its experimental validation. In Section 5, the co-optimization results are shown and analyzed. Finally, Section 6 will be dedicated for conclusions and perspectives of this work.

2. Modeling

In HTTES systems, a fan is used to push hot air through the porous medium as shown in Fig. 1(a) in order to charge the system with energy. The air (HTF) enters the storage through the hot section and gives up its heat to the storage materials (HSM). The heat exchange is done by convection between the fluid and the solid but also by conduction from one solid particle to another. Therefore, the storage medium heats up throughout the storage, creating what is called a thermocline that can be seen in Fig. 1(b). During the discharge process, the cold air enters the storage though the cold section and warms up thanks to the convective heat exchange with hot HSM. Here, multiple complexes heat transfer mechanisms occur such as convection, conduction and radiation between the three storage phases (solid, fluid and walls). To control the thermal charging power P_{sto} of such a system, the flow rate and entry air temperature are accordingly calculated. During the discharge process, cold air is blown into the storage, and its flow rate is calculated based on the outlet temperature, to reach the desired

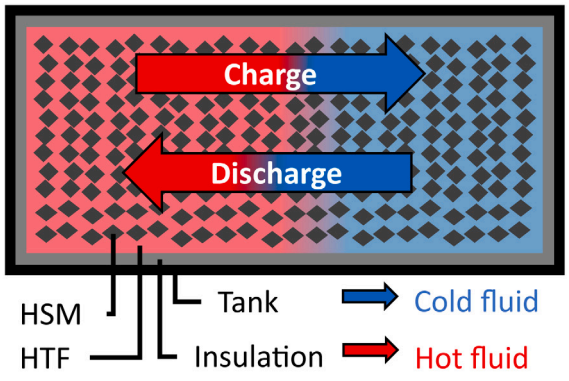

(a) Illustration of HTTES main components and HTF flow direction during the charge and discharge process.

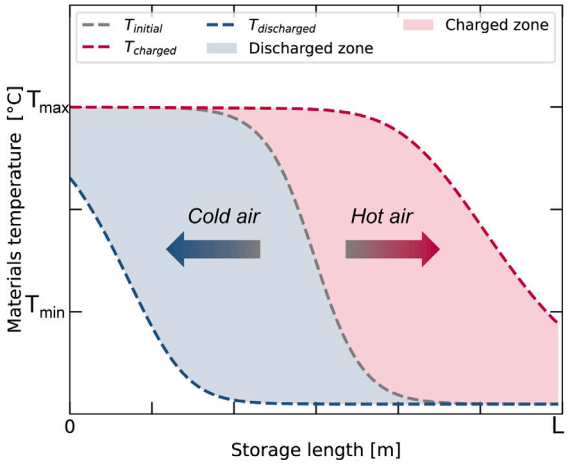

(b) Evolution of HSM temperature along the storage length during charging and discharging phase.

Fig. 1. HTTES simplified illustration.

thermal discharging power. In order to estimate the storage energy evolution, an energy balance can be applied using the HSM temperature. System losses can be divided into loss at walls and charging phase loss. In fact, when charging the system, the outlet temperature of the storage increases. Therefore, the charging phase air leaving the system, contains residual heat that is being lost into the atmosphere.

As said before, the predictive controller used to operate optimally the storage needs a model to estimate the system behavior. Here, the storage energy state and losses evolution in function of the power command are required for the controller to design and manage the system. This section will be dedicated for describing two 0D models, a 1D based on PDE model as well as a 1D metamodel as explained in [8], whereas 2D models are out of the scope of this work.

2.1. Accurate model: 1D - PDE

In this work, 1D - PDE represents the most accurate model in the scope of this work. It solves PDE on the fluid (HTF) but also the two solid phases (HSM and walls) respecting the energy conservation principle. As a results, the temperature evolution can be obtained accordingly to time and to one spacial dimension (length of the storage). Here below the heat equations taking into account the convection, conduction and fluid advection phenomena :

- Fluid :

$$\varepsilon \left(\rho c_p\right)_f \left(\frac{\partial T_f}{\partial t} + u\frac{\partial T_f}{\partial x}\right) = k_f^{\text{eff}} \frac{\partial^2 T_f}{\partial x^2} + h_v(T_s - T_f) + h_w \frac{A_{f\leftrightarrow w}}{V_f + V_s}(T_w - T_f) \tag{1a}$$

- Solid :

$$(1-\varepsilon)\left(\rho c_p\right)_s \frac{\partial T_s}{\partial t} = k_s^{\text{eff}} \frac{\partial^2 T_s}{\partial x^2} + h_v(T_f - T_s) + h_w \frac{A_{s\leftrightarrow w}}{V_f + V_s}(T_w - T_s) \tag{1b}$$

- Wall :

$$\left(\rho c_p\right)_w \frac{\partial T_w}{\partial t} = k_w \frac{\partial^2 T_w}{\partial x^2} + h_{\text{ext}} \frac{A_{w\leftrightarrow \text{ext}}}{V_w}(T_{\text{ext}} - T_w) + h_w \left(\frac{A_{f\leftrightarrow w}}{V_w}(T_f - T_w) + \frac{A_{s\leftrightarrow w}}{V_w}(T_s - T_w)\right) \tag{1c}$$

Physical proprieties as well as correlations for effective thermal conductivities and heat transfer coefficients are presented in Appendix. Solving numerically PDE on the three phases, using finite difference method, results in the evolution of the storage temperature. Later on, the energy evolution and the losses of the system, based on the obtained temperature, can be calculated using Eqs. (2a) and (2b). More information on how to calculate the Eqs. (1a), (1b) and (1c) parameters can be found in [13,16,18].

$$E_{sto} = (1-\varepsilon) S_{bed} \cdot \rho_s \int_0^L c_p^s(x)\Big(T_s(x) - T_{ext}\Big)\mathrm{d}x \tag{2a}$$

$$P_{loss-ch} = \begin{cases} 0 & \text{if } T_{outlet} = T_{ext} \\ \dot{m} \cdot c_p^f (T_{outlet} - T_{ext}) & \text{if } T_{outlet} > T_{ext} \end{cases} \tag{2b}$$

This model has the highest computation time compared to other models in the scope of this work (approximately 1 to 10 s for the simulation of one hour of the storage operation). Hence, this model is not suitable for use in an optimization controller. Further information on models computation time can be found in Section 4.

2.2. Ideal storage: 0D - ideal

In 0D - Ideal models, the losses before saturation are completely neglected. This means that all the injected energy into the system is being stored. In other words, heat transfer between fluid and solid is supposed to be perfect and instant, and heat transfer to walls is completely neglected. As a results, the thermocline (temperature gradient) which is the zone where the HSM temperature varies is null. The dynamics of the system according to this model can be expressed as follows:

$$E_{sto}^{t+\Delta t} = E_{sto}^t + \Delta t \cdot P_{sto}^t \tag{3a}$$

$$P_{loss}^t = \begin{cases} 0 & \text{if } E_{sto}^t < E_{rated} \\ P_{sto}^t & \text{if } E_{sto}^t = E_{rated} \end{cases} \tag{3b}$$

where E_{rated} is the maximum storage capacity.

Storage heat losses are zero at all times except when the system is charged even though it is already fully charged and can be calculated as expressed here above. The advantage of such a model is the low computation time that comes with rough heat transfer and losses assumptions.

2.3. Uniform temperature storage: 0D - uniform

0D - Uniform models assume the same temperature value T_{mean} for the whole HSM. This means that the thermocline zone covers the whole

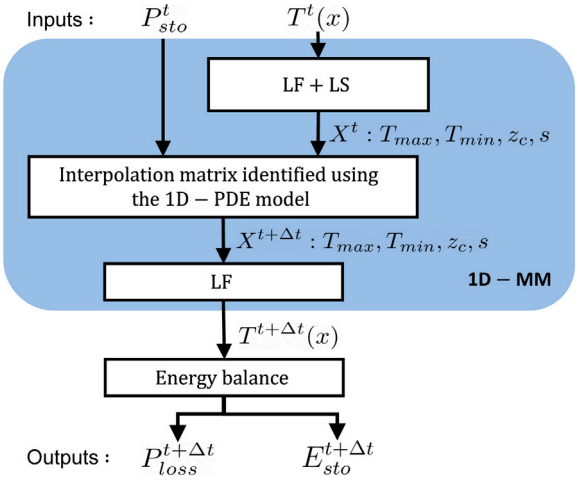

Fig. 2. Illustration of the inputs, outputs and the main activated tasks when running the metamodel. LF : Logistic Function, LS : Least Square algorithm.

storage length. This temperature can be calculated using Eq. (4c). In such a model, energy evolution and losses, based on T_{mean}, are expressed in Eq. (4a) and (4b).

$$E^{t+\Delta t}_{sto} = E^t_{sto} + \Delta t \cdot P^t_{sto} - \Delta t \cdot P_{loss}(T^t_{mean}, \dot{m}) \tag{4a}$$

with $$P^t_{loss} = \dot{m} \cdot c^f_p (T^t_{mean} - T_{ext}) \tag{4b}$$

and $$T^t_{mean} = \frac{E^t_{sto}}{c^s_p m} + T_{ext} \tag{4c}$$

Concerning losses, only the charging phase heat losses are being considered in this model. This model does not consider the second aspect of loss, the loss at walls, unlike 1D models. This model comes with low computation time but overestimates losses and has inaccurate representation of the storage temperature. This explains their frequent use in TES optimization work and their limitation to achieve feasible optimal design and management strategy. Consequently, a trade-off model is required to optimize design and management of TES with acceptable computation time.

2.4. Metamodel: 1D - MM

This subsection presents the metamodeling approach, based on a 1D - PDE model simulations, that has been developed in [8]. Depending on the initial storage temperature $T^t(x)$ and the power command P_{sto}, it is possible to calculate the evolution of the storage temperature $T^{t+\Delta t}(x)$ after a fixed period of time Δt. Later on, the storage energy and losses can be deduced by applying Eq. (2a) and (2b). Thanks to an analytical approximation based on a pre-built information matrix, 1D - MM is able to estimate the temporal evolution of the HSM temperature along the storage length. Fig. 2 illustrated the main calculation steps in the metamodel. 1D - MM showed a trade-off between accuracy and computation time as discussed in [8], thanks to the pre-built matrix that avoids solving PDE in the simulation stage. Therefore, it seems adequate to use 1D - MM inside a predictive controller, which will be the subject of next sections in this work.

The temperature spacial approximation in the metamodel is achieved by applying a least square algorithm to estimate the logistic function parameters described in Eq. (5).

$$T(x, T_{max}, T_{min}, z_c, s) = T_{max} + \frac{T_{max} - T_{min}}{1 + e^{(x - z_c)/s}} \tag{5}$$

The temporal approximation used to estimate the final state, starting from an initial state, is a linear interpolation based on a pre-built matrix. The construction of the information matrix use 1D - PDE

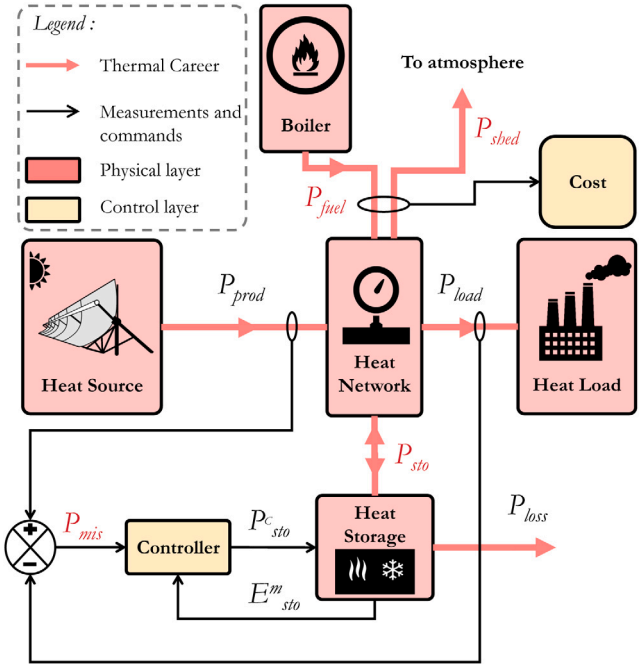

Fig. 3. Synopsis of the reference case study.

simulations data as shown in algorithm 1. This step can be time consuming depending on the discretization level of the logistic function parameters (T_{min}, T_{max}, z_c, s) as well as the power command P_{sto}. On the other hand, a higher discretization level signifies higher accuracy for the metamodel as finer temporal approximation can be achieved. Therefore, it is necessary to find the best trade-off between accuracy and computation time. Here we will call i the discretization of logistic function parameters and j the discretization of the power command. All along this work, two metamodels will be investigated. A first one with low discretization level called 1D - MM^{3,7} ($i = 3$ and $j = 7$) and another with high discretization level called 1D - MM^{7,15} ($i = 7$ and $j = 15$). More details on the metamodel can be found in [8]. The next subsection compares the computation time between the discussed models.

Algorithm 1: Procedure for the construction of the metamodel identification matrix.

Data: $T^t_{min} \in \boldsymbol{T_{min}}, T^t_{max} \in \boldsymbol{T_{max}}, z^t_c \in \boldsymbol{z_c}, s^t \in \boldsymbol{s}, P^t_{sto} \in \boldsymbol{P_{sto}}$

Result: $f : X^t; P^t \longmapsto X^{t+\Delta t}$

with $X^{t+\Delta t} = [T^{t+\Delta t}_{min}, T^{t+\Delta t}_{max}, z^{t+\Delta t}_c, s^{t+\Delta t}]$
and $X^t = [T^t_{min}, T^t_{max}, z^t_c, s^t]$
initialization;
foreach $T^t_{min}, T^t_{max}, z^t_c, s^t$ **do**
  foreach P^t_{sto} **do**
    calculate $T^t(x)$ with Eq. (5)
    calculate $T^{t+\Delta t}(x)$ by solving Eq. (1a) (1b) (1c)
    calculate $T^{t+\Delta t}_{min}, T^{t+\Delta t}_{max}, z^{t+\Delta t}_c, s^{t+\Delta t}$ with Eq. (5) and least square algorithm
  end
end

3. Description of case study

The goal of this work is to study the sensitivity of HTTES co-optimization results to model choice in terms of controller performance and computation time, for different business models. Here, studied

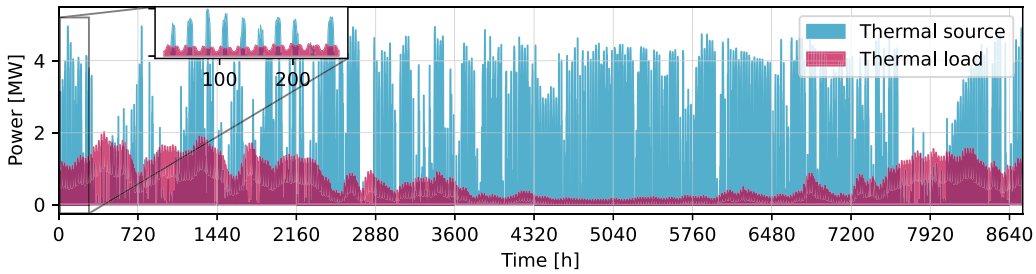

Fig. 4. Power time series for thermal source and load. In blue is the thermal source power issued from 5500 m^2 CSP field in the south of France, with a total annual production of 7 500 MWh. In pink is the load power consumed by 2 MW industry in France, with a total annual consumption of 5 000 MWh. All data corresponds to 2013 and can be found in [32,34].

models consider storage losses more or less accurately as described in Section 2. Therefore, two business models have been formulated to compare the obtained results in case that losses are counted or not in the objective function. Indeed to calculate losses accurately, local information such as outlet temperature needs to be estimated which is the case of multi-energy networks. Here, the case study includes a thermal carrier with two sources and one load as this would be sufficient to study the HTTES co-optimization sensitivity to models. The case study used for the optimization work is presented in Fig. 3. The consumed thermal power P_{load} is given by [32], an aggregated estimation of consumed thermal power by heat networks in France in 2013. Based on those data, the load is supposed to be an industrial with a thermal peak load of 2 MW that consumes a total of 5000 MWh per year. As shown in Fig. 3, this case study includes a main source which is a fuel boiler P_{fuel} to cover the load. Additionally, a renewable production source of 5500 square meters concentrated solar power (CSP) field will be connected in order to avoid fuel consumption. This source is composed of heliostat mirrors and thermal receiver tower as described in [33], with a total production of 7500 MWh per year and a production peak of 5 MW. The solar data for the direct normal irradiation (DNI) is issued from PVGIS database developed by the European commission [34], and correspond to the Occitania region in the south of France in 2013. The thermal output of the central is calculated using Eq. (6).

$$P_{prod}(t) = \eta_{hel}(t) \cdot S_{hel} \cdot DNI(t) \tag{6a}$$

$$\text{with} \quad \eta_{hel} = \rho_{ref} \cdot \eta_{tra} \cdot cos\theta \cdot \eta_{sh} \cdot \eta_{blo} \cdot \eta_{spil} \tag{6b}$$

where P_{prod} is the CSP field thermal produced power, η_{hel} is the instantaneous optical efficiency of the heliostat field, S_{hel} is the reflective area (here 5500 m^2), DNI is the direct normal irradiation, ρ_{ref} is the heliostat reflectivity, η_{tra} is the atmospheric transmission between the heliostat and the receiver, $cos\theta$ is the cosine of the angle formed between the normal to the heliostat surface and the incident rays, η_{sh} is the fraction of the heliostat surface shaded by adjacent heliostats, η_{blo} is the fraction of the reflected sunlight blocked by adjacent heliostats and η_{spil} refers to the fraction of reflected sunlight missing the receiver due to other technological errors. For simplicity, η_{hel} is assumed constant and equal to 0.9. In addition, HTTES is considered with charge and discharge thermal power P_{sto}. As a result, the storage flexibility would help the CSP energy to meet the considered load and so that allows further reduction in boiler fuel consumption. Here, thermal sources, load and storage system are supposed to be on high temperature of 600 °C. It is to be noticed that, the only considered power loss in this case in the heat storage losses (losses from heat network and others are not considered). Both production and load time series can be visualized over a year in Fig. 4.

The goal of this case study is to optimize the management of the thermal storage for different design points in order to minimize the objective function. Two objective functions are studied here and correspond to two different business models (BM). In the first one, only the call on the main boiler P_{fuel} in case of overconsumption is to be minimized over a year without paying the losses related to the storage system. In the second one, thermal losses linked to storage P_{loss} is to be minimized also with the call on the boiler which mean that the storage operator pays the losses also. This problem is deterministic and subject to physical constraints which are explained in Eq. (7).

$$\min \sum_{t=i}^{n_w} C_{tot}(t) \tag{7a}$$

$$\text{where } C_{tot} = \begin{cases} P_{fuel} \cdot \Delta t, & \text{for BM } n^o1 \\ (P_{fuel} + P_{loss}) \cdot \Delta t, & \text{for BM } n^o2 \end{cases} \tag{7b}$$

$$\text{with } P_{mis}(t) - P_{sto}(t) + P_{fuel}(t) - P_{shed}(t) = 0 \tag{7c}$$

$$P_{mis}(t) = P_{prod}(t) - P_{load}(t) \tag{7d}$$

$$0 \le P_{fuel}(t) \text{ and } 0 \le P_{shed}(t) \tag{7e}$$

$$-P_{rated} \le P_{sto}(t) \le P_{rated} \tag{7f}$$

$$0 \le E_{sto}(t) \le E_{rated} \tag{7g}$$

$$P_{rated} = E_{rated} \tag{7h}$$

It is to be noticed that P_{sto} follows a receptor convention: P_{sto} has a positive sign when charging and negative when discharging. The storage dynamics reflecting storage energy E_{sto} and heat loss P_{loss} evolution in function of the storage command P_{sto} are estimated using one of the four models described in the previous sections. The problem is solved numerically using Model Predictive Control (MPC) as described in algorithm 2. The time horizon N of the resolution is 8760 h. At each time step (here $\Delta t = 1$ h), an optimization problem is formulated and solved on a sliding window of size n_w. Only the first sample of the output sequence is implemented for simulation, subsequently the sliding window is shifted of 1 h. Within the present simulation framework, the new state of the system at the next time step is estimated by the accurate model 1D - PDE simulation, which is considered as a reference. Then a new optimization problem is solved using this new information. In whole work, the accurate 1D - PDE model is the only model used for simulation and estimation of the real system energy state and losses. It is to be noticed that investigated HTTES capacities are ranging from 2 to 20 MWh$_{th}$. This choice has been made based on the HTTES studied technology which is adapted for daily to weekly cycles but not for seasonal storage purpose. This means that a part of fuel consumption is not replaceable as more load appears in winter period, oppositely to CSP production that is more important in summer period as shown in Fig. 4. In other words, a seasonal storage would be needed to cover the totality of the heat consumption in this case study — which is out of this work scope. Otherwise, an irreducible residual consumption is unavoidable.

4. Simulation models discussion

The goal of this section is to validate the studied models for simulation purposes and to evaluate their committed errors. This step is necessary before beginning the co-optimization work. Indeed, HTTES

Algorithm 2: MPC description

Data: n_w, N

Result: $\min \sum_{i=0}^{N} \sum_{t=i}^{i+n_w} C_{tot}(t)$

initialization;

for i in N **do**

  calculate $\langle \boldsymbol{P}_{sto} \rangle_{n_w}$ by solving Eq. (7) using a model in Table 1 ;

  simulate $P_{sto}[0]$ with 1D - PDE model ;

  calculate $P_{fuel}(t) + P_{loss}(t)$ and energy balance with Eq. (2a)

end

installations can be divided into two categories; installations that fit with 1D - PDE assumptions and installations presenting manufacturing defects, aging or highly dimension-dependent phenomena like flow channeling.

4.1. Standard HTTES models validation

In most designs, 1D - PDE reproduces faithfully the real system behavior, except in certain configurations as described in [8]. In general, this is the case of large scale HTTES without manufacturing defects. An alternative could be the 1D - MM based on 1D - PDE simulations data which is accurate and divides the computation time by a 1000 factor. Also, 0D models can be used to estimate storage energy evolution with low computation time but not local variable such as storage outlet temperature. Here, we will study, on the basis of a year optimal command simulation, the evolution of the HTTES energy based on four models. 1D - PDE is supposed to reproduce faithfully the real storage energy evolution. Hence, the 1D - PDE simulation results will be compared to the four models, listed in Table 1, to calculate each model error. For this purpose, an example of 20 MWh capacity HTTES is used to conduct simulations and evaluate models errors.

Fig. 5 shows the evolution of the storage energy over a year with a time step of 1 h. Also, the relative error as well as the normalized root mean square deviation (NRMSD) (defined in [8]), between studied models and 1D - PDE are illustrated. Indeed the NRMSD error has been selected as a metric in order to sidestep calculation problems that appear when investigated values are near from zero. It can be defined as :

$$\text{NRMSD} = \frac{\text{RMSD}}{x_{max} - x_{min}} \tag{8a}$$

$$\text{with} \quad \text{RMSD} = \sqrt{\frac{\sum_{i=0}^{n} (x_i^{exp} - x_i^{model})^2}{n}} \tag{8b}$$

where x_{max} and x_{min} are the maximum and minimum in the investigated numerical values, respectively and n is the sample size.

Results show that for 0D models, errors are mostly committed when battery is near from saturation. This can be explained by the fact that, 0D models assumptions estimate poorly the outlet temperature. Therefore, losses during the charge phase, that are mostly present in energy levels near saturation, are underestimated in 0D - Ideal and overestimated in 0D - Uniform. It is to be noticed that 1D - MM^{3,7} that is poorly discretized, commits more errors than 0D models in mean. Therefore, it is important to find the best trade-off of discretization in terms of computation time and accuracy for metamodels. Furthermore, the error committed by 1D - MM^{7,15} is the lowest error as it represents faithfully the 1D - PDE. NRMSD values for 0D - Ideal, 0D - Uniform, 1D - MM^{3,7} and 1D - MM^{7,15} can be visualized in Table 1. N_{cons} stands for the number of simulation iterations, and t_{cons} for the computation time, to build the metamodel information matrix. The model computation time to simulate one hour of storage operation will be called t_{sim}. In this example, the 1D - MM allows to reduce the computation time by a factor of 1000 for simulation purposes, compared to the 1D - PDE model. As a result, for storage systems without defects, 1D - MM^{7,15} shows high accuracy with suitable computation time as well as the ability to estimate local variables of HTTES. This can be an alternative for 1D - PDE, in co-optimization work, that is accurate but time consuming.

Table 1
Summary of studied models simulation performance in terms of computation time and NRMSD error. The NRMSD concerns the storage energy evolution over a year of operation, and has been calculated relatively to 1D - PDE results.

Model	N_{cons}	t_{cons} [s]	t_{sim} [s][a]	NRMSD [%]
0D - Ideal	–	–	< 0.001	8
0D - Uniform	–	–	< 0.001	13
1D - MM^{3,7}	567	600	≈ 0.001	15
1D - MM^{7,15}	36 015	36 000	≈ 0.001	3
1D - PDE	–	–	1 – 10	–

[a] *Intel® Core i7-6820HQ CPU @ 2.70* GHz.

4.2. Defected HTTES models validation

As the construction of a HTTES is not an easy task, it can happen that the behavior of a real infrastructure does not correspond to the 1D - PDE model. This may result from imperfections during the construction such as non homogeneous air distribution, increased wall effects, manufacturing defects or material aging particularly in small scale installations. Such flaws could undermine the effectiveness of the whole co-optimization approach, since the behavior of the actual infrastructure could no longer be anticipated before implementation. Thus, this paragraph presents how a metamodel can be built from experimental tests on an installation with defects. The accuracy evolution of such a model can be estimated in function of the number of experimental tests and measurement frequency as described in [8]. This subsection will investigate the construction of such a model and evaluate its performance based on real experimental data and will compare its performance to 1D - PDE in this configuration.

On the one hand, this allows for the optimal control of an installation that cannot be modeled analytically. Moreover, in an operational co-optimization approach, an analysis of the risks related to such defects could be taken into account.

Fig. 6 describes the HTTES facility studied in this work. This installation is classified as high-temperature unpressurized air/rock packed-bed storage, where atmospheric air is used as heat transfer fluid (HTF) and rocks as heat storage material (HSM). Further more, the packed bed has a horizontal cylindrical geometry with a maximum storage capacity E_{max} of 40 kWh_{th} (calculated for an ambient temperature of 0 °C). $P_{CH,max}$ and $P_{DC,max}$ are the maximum charge and discharge power, here equal to 27.6 and 37.6 kW_{th} respectively. The presented installation is a prototype that has been developed by the company Eco-Tech CERAM for material characterization purpose and innovative thermal storage applications validation. In this work, the facility has been connected to an electrical heater as shown in Fig. 6(a). The storage is composed of a metallic cylinder that encapsulated insulation and the HSM. The HTTES is equipped with a total of 29 temperature sensors of which 9 are along the central axis of the unit distributed over the sections named A and B, as shown in Fig. 6(b). To avoid wall effects, only temperatures date from the 9 central axis sensors will be used. A summary of the main characteristics of the HTTES, such as the bed diameter D_{bed}, length L_{bed}, volume V_{bed}, particle diameter D_p, storage maximum temperature $T_{storage,max}$ can be found in Table 2. It is to be mentioned that the whole installation has been adapted to receive real-time commands remotely passing by a virtual private network. This applies for all registers, heater and fan. Also, all measures are recorded in real time on a remote data base.

Since this HTTES facility is of small capacity and has been operating under extreme conditions for more than 5 years, its behavior differs

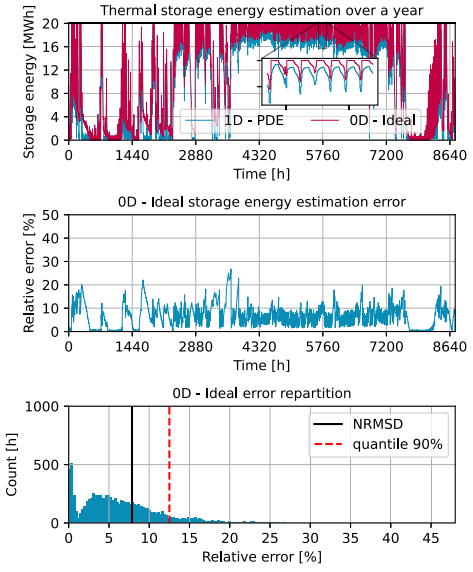

(a) 0D - Ideal compared to 1D - PDE

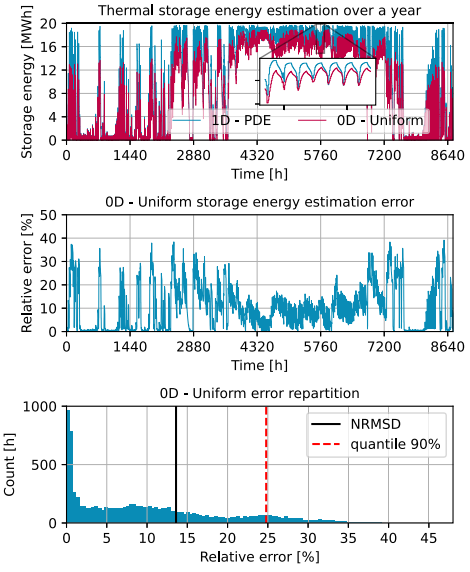

(b) 0D - Uniform compared to 1D - PDE

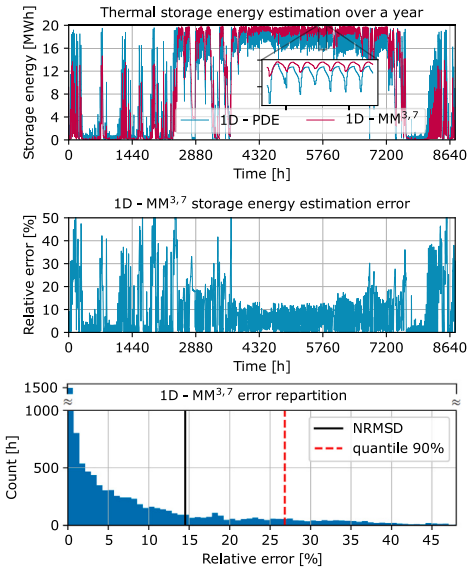

(c) 1D - $MM^{3,7}$ compared to 1D - PDE

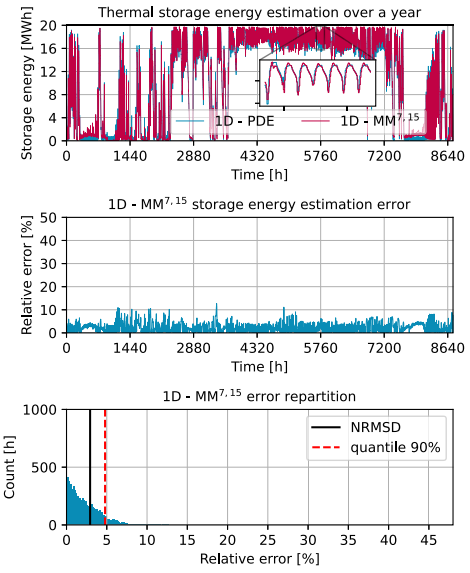

(d) 1D - $MM^{7,15}$ compared to 1D - PDE

Fig. 5. Simulation results of an optimal management issued from four investigated models and compared to 1D - PDE for a 20 MWh storage. Results show the evolution of the storage energy estimation and the error between the investigated model and the accurate 1D - PDE over a year.

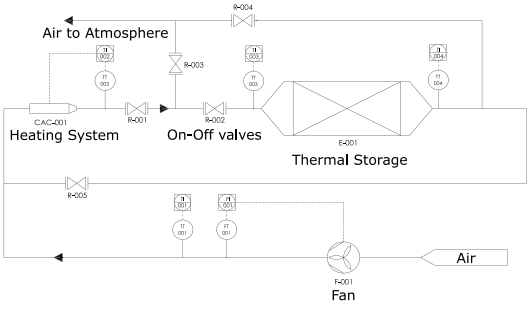

(a) Process flow diagram

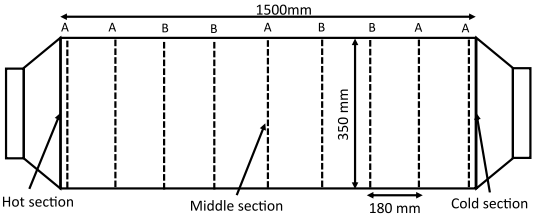

(b) Location of temperature sensors inside the storage. Considered sensors are those in the center of sections named A and B.

Fig. 6. Description of the HTTES facility from Eco-Tech Ceram.

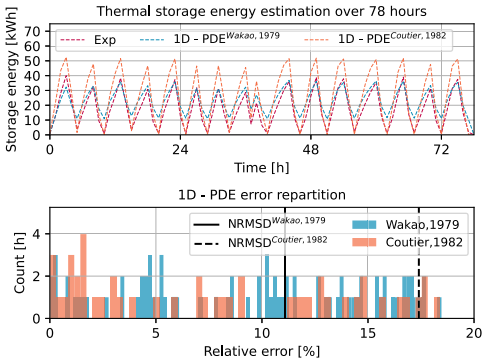

(a) 1D - PDE models simulations and experimental measured data comparison

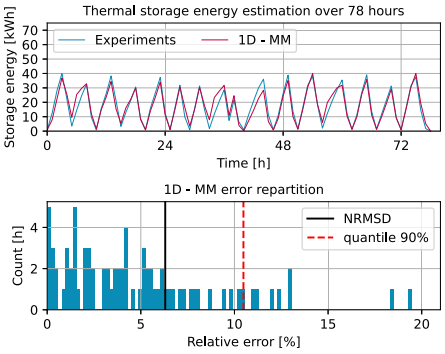

(b) 1D - MM model simulation and experimental measured data comparison

Fig. 7. Simulation results of an optimal management, issued from two 1D - PDE models and 1D - MM, compared to experimental test data for a 40 kWh test facility. 1D - PDE models use different correlations for h_v coefficient as described in Appendix. The 1D - MM used in this figure is a metamodel built on experimental results measured for previous experiments explained in Table 3. Results show the evolution of the storage energy estimation and the error between investigated models and the experimental data over 78 hours experiment.

Table 2
Summary of the HTTES prototype characteristics used for conducting experimental tests.

Geometry	Flow	HTF	HSM	D_{bed} [m]	L_{bed} [m]	V_{bed} [m^3]	D_p [mm]	E_{max} [kWh$_{th}$]	$T_{storage,max}$ [°C]	$P_{CH,max}$ [kW]	$P_{DC,max}$ [kW]	ϵ	Sensors used
Cylindrical	Horizontal	Air	rocks	0.35	1.5	0.144	30	40	575	27.6	37.6	0.425	9

from hypothesis supposed by most of literature models. This is due to important air leakage and preferential passages that become more important in small scale designs and which are not modeled neither in 1D - PDE nor in 0D models. In fact, energy balance has been calculated on the basis of the installation measures. This showed that, nearly 35% (in average) of the energy consumed by the heating system is not being transferred to the storage, during the charge phase. Although losses through the outlet section during the charging phase has been accounted for, this energy difference is still being observed. After several verification by the mean of measuring instruments and mass balance, an important hot air leakage has been confirmed and located upstream of the storage inlet. It is to be noticed that other source of errors can impact the accuracy of the 1D - PDE model. Moreover, model correlations choice can be another source of errors. The impact of HTTES model correlations choice has been discussed partially in some research work [18,35]. In general, results show that models are poorly sensitive to heat transfer coefficient with the outside and between walls and other components. However, heat transfer coefficient between solid and fluid h_v can has an important impact on the model results. Hence, 0D - Ideal, 0D - Uniform, and two 1D - PDE models have been used to simulate the behavior of the studied facility using an optimal management command over 78 h. Each 1D - PDE model use a different correlation for h_v coefficient as shown in Appendix. The first 1D - PDE model uses Wakao, 1979 [36] correlation where the second one uses Coutier, 1982 one [37]. A sample of models results, only for the two 1D - PDE models are shown in Fig. 7(a). It shows high discrepancy between both models and experimental results. Indeed, the first correlation underestimates the heat transfer efficiency, compared to experiments, whereas the second one overestimates it. In terms of NRMSD, the scores values are 12, 17, 13 and 30%, for 1D - PDE (Wakao, 1979), 1D - PDE (Coutier, 1982), 0D - Uniform and 0D - Ideal respectively. In the following, we will focus on the metamodeling approach when physical defects occur and lead to important discrepancies between experience and models results, independently of the choice of the models correlations.

To address this limitation, this same installation is being used to conduct four experimental tests, with full charging and discharging cycles. Those tests results will be used to construct the 1D - MM based on experimental measured data with variable power commands and fixed measurement frequency as illustrated in Table 3. Once the experiments are conducted, the data collected and treated, and then the 1D - MM can be constructed. Afterward, this model is used to simulate an optimal management command over 78 h, which is also being applied on the same test facility in order to evaluate the performance of the constructed model. Fig. 7(b) shows the evolution of the storage energy level for both experimental data and the 1D - MM based on experiments as well as the error of the model. It is to be noticed that the NRMSD value is slightly higher than 6%, which is near from values estimated by [8]. Also, this 1D - MM has higher accuracy than the three other investigated models studied here.

Table 3
Summary of the different conducted experimental tests for the metamodel construction.

Test number	1	2	3	4
Charge power [kW]	13.4	18.15	22.87	27.6
Discharge power [kW]	20	25.87	31.74	37.6
Test duration [h:m]	8:15	6:32	5:38	5:00
Measurement period [s]	60	60	60	60

As a consequence, metamodeling based on experience can replace physical equation based models in case of defected installations or specific designs. This section showed that 1D - PDE and 1D - MM can be used to simulate non defected large scale HTTES installations in the designing phase. On the other hand, experimental based metamodels can be used to simulate or optimize management of existing defected or small scale HTTES installations. In the next section, we will admit 1D - PDE as a simulation model to conduct co-optimization work, in the design phase, on a unique accurate base. All investigated installations in the next section are supposed to be without manufacturing defects.

5. Co-optimization

The goal of this section is to select appropriate controller model for co-optimization work based on two business models. The first BM does not count losses while the second one does. This aims to distinguish the impact of models on co-optimization when taking into account losses or not. The optimization model performance evaluation will be based on a physical metric that will be presented later in this section. All along

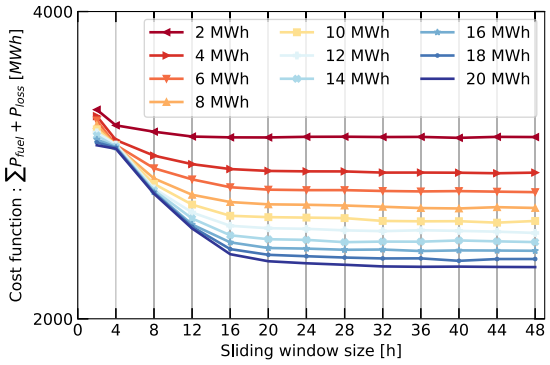

Fig. 8. Evolution of the cost function, with 0D - Uniform as optimization model and 1D - PDE as simulation model, according to increasing sliding window size. Curves correspond to investigated storage capacities.

this work, simulation and optimization models will be distinguished. In fact, 1D - PDE model will be used along this work to simulate the optimization results in order to verify the accuracy of the calculated optimal commands. The choice of the 1D - PDE is motivated by the fact that real system behavior is reproduced faithfully by this model in most designs especially for large scale storages [8] – except regarding defaults as discussed Section 4.2. The studied optimization models are : 0D - Ideal, 0D - Uniform, 1D - MM^{3,7} and 1D - MM^{7,15}. Moreover, a study for sliding window size n_w selection in function of the storage capacity will be conducted. Based on the obtained results, the minimum accepted size (the size from which the cost function converges to an asymptote) can be decided for each capacity in order to limit the calculation time. In the rest of this work, the optimization is coded in Python language and uses SciPy library [38]. A summary of all models in the scope of this study are described in Table 1. It is to be noted that Sequential Least Squares Programming (SLSQP) optimization algorithm from SciPy library has been used to solve the minimization problem along this work.

5.1. Identification of sliding window size

For this part, 0D - Uniform model is used to solve the MPC problem over 8760 h with different sliding window sizes as shown in Fig. 8. For each capacity, the smallest window size is chosen, ensuring the minimum value of the cost function with 5 % tolerance. Results shows a faster convergence of the cost function for small battery capacities. This can be explained by the fact that for small storage capacity, saturation is reached earlier. Therefore, future events anticipation has lower weight in the cost function. The sliding window size selected for the rest of this study is fixed on 24 h. This choice is made as it is the smallest window size (less time consuming) that guarantees convergence of cost function values for all studied capacities.

5.2. Results discussion and analysis

In this subsection, four models (as described in Table 1) of increasing accuracy will be used for the optimization process while only 1D - PDE will be used for the simulation of the optimization results. As a reminder, the storage system operator in this study case has two business models. The first one aims to avoid the boiler fuel consumption only and the second one aims to avoid losses as well as boiler consumption as explained in Section 3. For each storage system design, multiple optimization models have been used to calculate an optimal management command. Once the command is obtained, the simulator is launched in order to evaluate the real system behavior according to the optimal command and to calculate the system life cost in terms of primary energy. In order to evaluate the model impact on both design and management results, multiple criteria can be used for this purpose. Here we focus on criteria that are based only on system energy costs without accounting for financial aspects. A first criteria can be the sum of the system primary energy costs over a fixed number of years. Those costs are equivalent to the cumulative energy demand (CED) and being calculated by the help of the tool developed by [10]. Here E_{design} is the CED needed for the storage construction, $E_{operating}$ is the CED needed to operate the storage system during a year of operation, E_{loss} is the CED of generated losses by the storage system over a year of operation, and E_{fuel} is the CED of consumed fuel that can be substituted thanks to the storage flexibility over a year of operation. It is to be noticed that losses are supposed to have the same CED value as the fuel per MWh of generated heat (here the fuel is natural gas with a CED of 1.215 MWh-*eq* per MWh of generated heat). Also, it is reminded that a residual consumption is unavoidable in the considered case study due to the absence of a seasonal storage. Then for the sake of readability of the results, only the boiler consumption E_{fuel} that can be substituted thanks to storage flexibility, will be visualized in the next figures as defined here below:

$$\textbf{System life cost} = E_{design} + (E_{fuel} + E_{operating} + E_{loss}) \cdot N^{years} \tag{9a}$$

$$\text{with } E_{fuel} = E_{fuel-saved_{max}} - E_{fuel-saved} \tag{9b}$$

where N^{years} is the operating period of the installation in years, $E_{fuel-saved_{max}}$ is the maximum yearly saved fuel when installing a 20 MWh$_{th}$ HTTES and optimizing management with the 1D - MM^{7,15} model (here equal to 1516 MWh/year) and $E_{fuel-saved}$ is the avoided fuel consumption over a year of operation of the investigated storage capacity.

Fig. 9 shows the evolution of the system cost components as a function of the storage installed capacity over a year of operation and for BM n°2 (with losses being taken into account in the objective function). This figure can be used to evaluate the performance of the controller and the obtained design if the HTTES relevance is evaluated over a one year period.

Fig. 9 shows high total life cost for the system controlled by a 0D - Ideal caused by important loss generation even though the fuel cost is well minimized compared to other models. This can be explained by the poor capacity of this model to estimate losses as it considers no loss before storage saturation. On the other hand, 0D - Uniform succeeds to limit losses, as this model overestimates the storage losses, but achieve a higher fuel consumption compared to metamodels results particularly when compared to 1D - MM^{7,15}. Optimal designs and total life cost values over a year of operating system for different models are illustrated on Fig. 9 with x symbols. Reductions of optimal costs are 30%, 20% and 14% when comparing 1D - MM^{7,15} to 0D - Ideal, 0D - Uniform and 1D - MM^{3,7} respectively. It is to be noticed that all models find near optimal designs around 10 MWh$_{th}$, except of 0D - Ideal that situates optimal design around 4 MWh$_{th}$ storage.

To investigate the impact of the facility's operating time, Fig. 10 shows the evolution of the sum of system life costs after multiple year operation for BM n°2 where 1D - MM^{7,15} has been used in the controller. The red dots shows the optimal designs that minimize the sum of system life costs, which are 12, 16 and 18 MWh$_{th}$ after 1, 2 and 4 years of operation respectively. It is be noticed that the optimal design changes in function of number of years of operation. In fact, the longer the length of operation, the higher the saved fuel cost, whereas the design cost is constant and independent of the operation length. This means that, for long term projections, optimal designs can have higher storage capacities compared to short term projections, which is the case here. Indeed, higher storage capacities (tending towards seasonal storage systems) are more profitable when storage operator is engaged for longer years of exploitation, but comes with higher risk (uncertainties linked to far future).

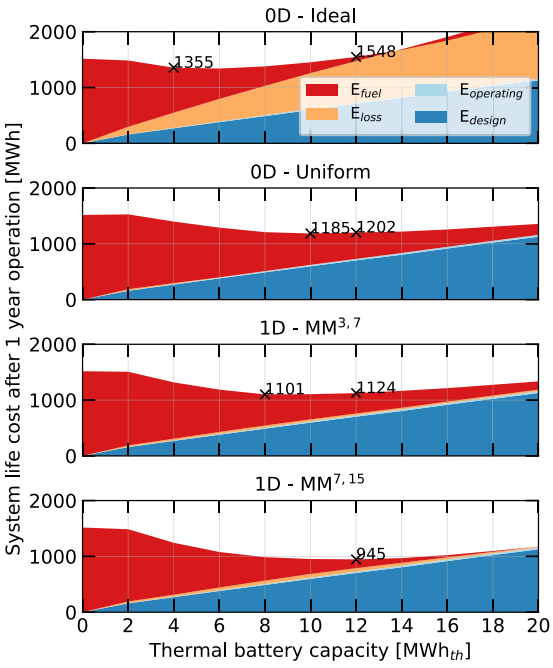

Fig. 9. Evolution of the system life cost components, after a year of exploitation, according to thermal storage installed capacity. Each sub figure refers to a system that has been operated with a controller using one of the four investigated models. x symbols on the plots indicates the minimum values of the system life cost after a year of operation and correspond to the optimal design.

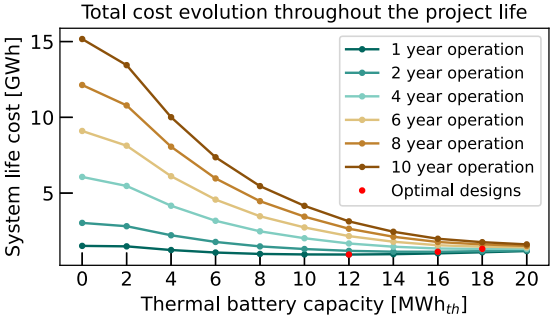

Fig. 10. Evolution of the sum of system life costs as a function of the installed storage capacity after different years of operation. Results are based on BM n°2 and issued from a controller that uses 1D - MM^{7,15} for co-optimization.

5.2.1. *Comparison between BM n°1 and BM n°2*

In order to discuss the difference between the two business models in a way that is independent of the length of operation, the Energy Payback Time (EPBT) is introduced in this section, as proposed in [10]. This criteria is used to calculate the time needed to payback the initial investment (here E_{design}), which allows to determine the storage capacity to install with shortest payback time as follows:

$$EPBT = \frac{E_{design}}{E_{fuel-saved} - E_{loss} - E_{operating}} \tag{10}$$

Here, for each design the EPBT criteria is evaluated as defined in Eq. (10). This criteria is calculated without taking into account the loss cost E_{loss} in BM n°1 and with loss cost in BM n°2. It is to be noticed that EPBT criteria, unlike the previous criteria, is adapted for high risk projects where the storage operator is engaged on short amount of time.

Figs. 11(a) and 11(b) show the evolution of EPBT in function of the storage installed capacity for each optimization model and for the two defined BM.

Fig. 11(a) for BM n°1 shows that all models, except 1D - MM^{3,7}, have similar controller performances and objective function minimized value. In mean, for all investigated storage capacities, 1D - MM^{3,7} increases the EPBT criteria by 5% as shown in Table 4. This is an illustration of the consequences of insufficient discretization when building a metamodel. Also, degraded model performance decreases (compared to other models) for large storage capacities. On the other hand, 0D models have similar management performances as 1D - MM^{7,15} for BM n°1, where objective function accounts only for fuel consumption without finer terms such as losses that depends on local system temperature values. Although 1D - MM^{3,7} has degraded performance, all models give the same optimal design situated around 4 MWh$_{th}$ storage. This shows that in case of BM n°1, where only fuel consumption is being taken into account in the objective function, simple and degraded models can be used to find the optimal design. However, degraded models do not succeed to reach other models optimal management performance.

As a comparison, regarding BM n°2, Fig. 11(b) shows that an increasing error can be observed for larger storage capacities when investigating the 0D - Ideal results. This can be explained by the poor estimation of generated losses, in 0D - Ideal, that is being taken into account in BM n°2. Those errors become more important as more losses are generated in large storage capacities. It is to be noticed that 1D - MM^{7,15} has the best optimal management score that other models could not reach. In mean, for all investigated storage capacities, the increase in EPBT criteria is 100, 25 and 14% for 0D - Ideal, 0D - Uniform and 1D - MM^{3,7} respectively compared to 1D - MM^{7,15}. On the other hand, the increase in optimal EPBT criteria is 35, 32 and 15% for 0D - Ideal, 0D - Uniform and 1D - MM^{3,7} respectively compared to 1D - MM^{7,15} as shown in Table 4. However, the decrease in models management performances, except for 0D - Ideal, does not prevent them from reaching the optimal design as they commit similar errors for all storage capacities. All models except 0D - Ideal reach similar optimal design around 6 MWh$_{th}$. Only 0D - Ideal reaches lower optimal design capacity around 4 MWh$_{th}$. The results show that for BM n°2, where losses are being taken into account, only models that consider global losses can reach the optimal design point. On the contrary, 0D - Ideal that only considers losses after storage saturation, fails to reach the optimal design. It is to be mentioned that metamodels results show improvements when they are more discretized (as described in Table 1) achieving better results for 1D - MM^{7,15}. In fact, larger state discretization vectors in metamodel lead to higher accuracy and lower approximations during the interpolation process. The limit of the discretization is governed by the choice of the logistic function used to approximate the storage temperature curve in the metamodel. Finally, it is to be mentioned that, the EPBT criteria for the optimal design does not increase significantly by accounting the storage losses. In effect, it is possible to apply an optimal management avoiding losses without decreasing significantly the saved gas amount thanks to storage flexibility.

5.2.2. *Simulation vs co-optimization performances*

As a reminder, Section 4 showed that 1D - MM^{7,15} have the best simulation performance score with an NRMSD lower than 3% when compared to 1D - PDE as shown in Table 1. Hence, the optimization scores achieved by 1D - MM^{7,15} are the best achieved scores in both BM n°1 and BM n°2. In BM n°1, 0D - Ideal as well as 0D - Uniform optimized EPBT remain very close from 1D - MM^{7,15} EPBT for almost all investigated capacities. This occurs although both 0D models commit non neglected errors in simulation process. On the other hand, 1D - MM^{3,7} commits the highest EPBT and NRMSD simulation errors. It seems that models which are able to estimate approximately the objective function terms (here storage energy level only for BM n°1) can be used for optimal design purposes. However, the more models are accurate in the storage energy simulation, the more management performance is improved. In BM n°2, 0D - Ideal fails to reach the optimal design as it does not consider storage losses before saturation.

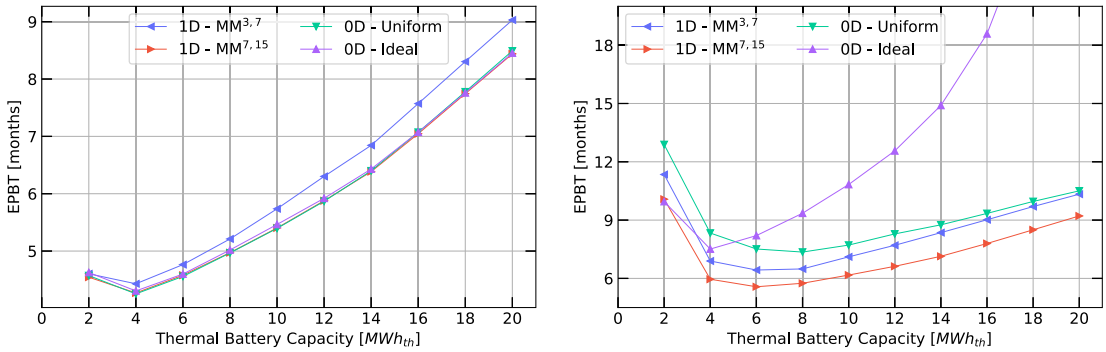

(a) EPBT results for BM n°1 : taking into account the fuel consumption without storage losses.

(b) EPBT results for BM n°2 : taking into account the fuel consumption with storage losses.

Fig. 11. Evolution of the Energy Pay Back Time (EPBT) according to battery capacity for BM n°1 and BM n°2. The optimization uses different models as described in the legend. The simulation of results is carried out by the physical model 1D - PDE.

Table 4
Summary of different models optimization performances. The increase in EPBT is calculated relatively to 1D - $MM^{7,15}$ EPBT that reaches the lowest values. t_{opt} is the computation time to solve the optimization problem over one hour using MPC algorithm as described in Section 3.

Models	Loss modeling [yes/no]	Local T modeling [yes/no]	t_{opt} [s]	Optimal design for BM n°1 [MWh_{th}]	EPBT increase for BM n°1 [%]	Optimal design for BM n°2 [MWh_{th}]	EPBT increase for BM n°2 [%]
0D - Ideal	no	no	≈1	4	<1	4	35
0D - Uniform	yes	no	≈1	4	<1	8	32
1D - $MM^{3,7}$	yes	yes	≈10	4	3	6	15
1D - $MM^{7,15}$	yes	yes	≈10	4	–	6	–
1D - PDE	yes	yes	>1500				

An important increase in EPBT can also be observed in the management performance, although it has an acceptable NRMSD simulation score. This shows that models which does not consider one of the objective function terms, are not able to find the optimal design and scores poor management performance. Other models that consider losses succeed to reach the optimal design and acceptable management scores even though those models commit important NRMSD simulation errors. In terms of simulation and optimization computation time, in average, 0D models are 10 times faster than metamodels, which are 100 to 1000 times faster than 1D - PDE as described in Tables 1 and 4. In other words, for objective functions such as BM n°1 where the goal is to optimize system-wide quantities, 0D models reach satisfying optimization scores compared to accurate 1D models with lower computation time. However, for finer objective functions such as BM n°2, 1D - $MM^{7,15}$ allows to reach a more optimal design and management score with greater but acceptable computation time.

6. Conclusions and perspectives

In this work, 5 models of increasing complexity level (0D - Ideal, 0D - Uniform, 2 metamodels and 1D - PDE), have been investigated. Those models have been confronted using a HTTES co-optimization problem, on the basis of a CSP energy source and industrial load over a year, where boiler fuel is to be avoided. Two BM have been studied, with and without considering losses generated by the HTTES. A simulation over a year has been carried out, where NRMSD has been calculated between each investigated model results and those of 1D - PDE (the latter is the most accurate model considered in this study). Results show that the metamodel that has high discretization level achieves the best NRMSD score lower than 3%.

Later on, a defected experimental setup is used to validate the models on the basis of real measurements. In this case it has been shown that all previously studied models fail to predict the behavior of such installation with NRMSD greater than 12%. However, a new metamodel constructed on the basis of real measurements, succeeds to predict the experimental setup behavior with NRMSD lower than 6%.

Furthermore, a co-optimization study has been conducted using the available models and for the two BM. A first optimal design evaluation using CED criteria has been conducted, over multiple operating periods. Results show that the longer the HTTES operating period, the greater is the optimal design capacity, with 12 and 18 MWh optimal capacities after 1 and 4 years of operation respectively. Therefore, it is more profitable to invest in greater storage capacities if storage operator is engaged over longer period, but this come with higher risk linked to unknown future events. Finally, a criteria called EPBT has been established for models performance comparison. BM n°1 shows that, when losses are not considered, all models succeed to reach the optimal design, but the most degraded model fails to reach the optimal management performance with an increase of 3% in the EPBT criteria for the latter. BM n°2 shows that, when losses are considered, models which consider losses succeed to predict the optimal design point but fails to achieve the same management performance as the highly discretized metamodel. In average over all investigated designs, an increase of EPBT criteria of 100, 25 and 14% for 0D - Ideal, 0D - Uniform and 1D - $MM^{3,7}$ respectively, can be observed compared to 1D - $MM^{7,15}$ EPBT values. Finally, the comparison between the 2 BM shows that, considering losses increases slightly the EPBT from 4.3 to 5.5 months, if co-optimized with appropriate model.

To summarize, we can distinguish three categories of models.

- First, models that consider all objective function terms with high accuracy. They reach the optimal design but also the optimal management score. This comes with considerable calculation time, in average 10 s per MPC iteration.
- Second, models that consider approximately all objective function terms. They reach the optimal design but score less optimal management. Generally, they have low computation time, in average 1 s per MPC iteration.
- Finally, models that do not consider all objective function terms. Those models fail to find the optimal design and management strategy.

In future work, multi-energies network could be considered to evaluate the model impact in such environment. Additionally, more

Table A.1
Summary of all correlations and physical proprieties used in this study 1D - PDE model. l_{wall} is the wall thickness, l_{iso} is the insulation layer thickness, *Re* and *Pr* are Reynolds and Prandtl numbers.

Parameter	Signification	Correlation/value	Choice justification	Reference
ρ_f [kg m^{-3}]	Air density	6.75E−18 T_f^6 - 2.429E−14 T_f^5 + 3.561E−11 T_f^4 - 2.799E−8 T_f^3 + 1.343E−5 T_f^2 - 0.004509 T_f + 1.274	Experimental measurements	[17]
c_{pf} [J kg^{-1} K^{-1}]	Air heat capacity	2.42E−10 T_f^4 - 7.131E−7 T_f^3 + 6.581E−4 T_f^2 - 8.615E−3 T_f + 1006	Experimental measurements	[17]
k_f [W m^{-1} K^{-1}]	Air thermal conductivity	9.38E−12 T_f^3 - 2.59E−8 T_f^2 + 7.30E−5 T_f + 2.477E−02	Experimental measurements	[17]
k_f^{eff} [W m^{-1} K^{-1}]	Air effective thermal conductivity	$\varepsilon \cdot k_f$	HTF conductivity in porous medium	[17]
ρ_s [kg m^{-3}]	Bauxite density	3005	Experimental measurements	[17]
c_{ps} [J kg^{-1} K^{-1}]	Bauxite heat capacity	8.890E−10 T_s^3 - 1.850E−6 T_s^2 + 1.531E−3 T_s^1 + 7.527E−1	Experimental measurements	[17]
k_s [W m^{-1} K^{-1}]	Bauxite thermal conductivity	−2.518E−9 T_s^3 + 5.423E−6 T_s^2 - 4.95E−3 T_s^1 + 5.070	Experimental measurements	[17]
k_s^{eff} [W m^{-1} K^{-1}]	Bauxite effective thermal conductivity	$(1-\varepsilon) \cdot k_s$	HSM conductivity in porous medium	[17]
ρ_w [kg m^{-3}]	Wall density	8070	Steel density	–
c_{pw} [J kg^{-1} K^{-1}]	Wall heat capacity	500	Steel heat capacity	–
k_w [W m^{-1} K^{-1}]	Wall thermal conductivity	18–45	Experimental measurements	[18]
$A_{f\leftrightarrow w}$[m^2]	Exchange surface between fluid and walls	$(\varepsilon)(\pi \cdot D_{bed} \cdot L_{bed} + (2\ \pi \cdot D_{bed}^2)/4)$	Exchange surface in porous medium	[35]
$A_{s\leftrightarrow w}$ [m^2]	Exchange surface between solid and walls	$(1-\varepsilon)(\pi \cdot D_{bed} \cdot L_{bed} + (2\ \pi \cdot D_{bed}^2)/4)$	Exchange surface in porous medium	[35]
$A_{w\leftrightarrow \text{ext}}$ [m^2]	Exchange surface between walls and outside	$\pi \cdot (D_{bed} + 2\ l_{wall}) \cdot L_{bed} + (2\ \pi \cdot (D_{bed} + 2 \cdot l_{wall})^2)/4$	Exchange surface in porous medium	[35]
h_v [W m^{-3} K^{-1}]	Heat transfer coefficient between fluid and solid	$(2+1.1 Re^{0.6} Pr^{0.33}) k_f / D_p$ $(700(\rho_f \cdot u/D_p)^{0.76}$	Models that takes into account inter-particle diffusion and adapted for air-solid bed	Wakao and Funazkri, 1979 [36] Coutier and Farber, 1982 [37]
h_w [W m^{-2} K^{-1}]	Heat transfer coefficient between walls and bed	$(0.203 Re^{0.33} Pr^{0.33} + 0.220 Re^{0.8} Pr^{0.4}) k_f / D_p$	Adapted for near-wall zone air-solid bed with spherical particles and with *Re*>40	Beek, 1962 [18]
h_{ext} [W m^{-2} K^{-1}]	Global heat transfer coefficient between walls and outside	$\frac{1}{A_{w\leftrightarrow \text{ext}}} \cdot \frac{1}{\frac{\log \frac{D_{bed}+l_{wall}+l_{iso}}{D_{bed}+l_{wall}}}{2\pi k_{iso} L_{bed}} + \frac{1}{h_{air} \cdot A_{w\leftrightarrow \text{ext}}}}$	Adapted for cylindrical packed bed	[35]
h_{air} [W m^{-2} K^{-1}]	Heat transfer coefficient between walls and outside air	$(0.664 Re_{air}^{0.5} Pr_{air}^{0.5}) k_{air} / L_{bed}$	Adapted for forced convection of an incompressible laminar air flow on a plane wall	[35]

sophisticated objective functions and business cases can be investigated for further comprehension of modeling impact on controller performance. Finally, the study of HTTES co-optimization under uncertainties is essential as it corresponds to real time management characteristics.

CRediT authorship contribution statement

Ibrahim Al Asmi: Conceptualization, Methodology, Data curation, Software, Validation, Writing – original draft, Visualization. **Roman Le Goff Latimier:** Conceptualization, Writing – review & editing, Supervision, Funding acquisition. **Yasmine Lalau:** Life-cycle assessment tools, data and review. **Thomas Brian:** Experimental setup and testing. **Hamid Ben Ahmed:** Writing – review & editing.

Declaration of competing interest

The authors declare that they have no known competing financial interests or personal relationships that could have appeared to influence the work reported in this paper.

Data availability

The data that has been used is confidential.

Acknowledgments

The authors would like to express their gratitude to the Association Nationale de la Recherche et de la Technologie (ANRT France 2018/1534) and the Danish Energy Technology Development and Demonstration Program (EUDP 64016-0027) for funding this work.

Appendix

See Table A.1.

References

[1] Paris-IEA, Greenhouse Gas Emissions from Energy Data Explorer, 2021, https://www.iea.org/articles/greenhouse-gas-emissions-from-energy-data-explorer.

[2] Eurostat, Energy consumption in households - Statistics Explained, 2020, https://ec.europa.eu/eurostat/statistics-explained/index.php.

[3] M. Mohammadi, Y. Noorollahi, B. Mohammadi-ivatloo, M. Hosseinzadeh, H. Yousefi, S.T. Khorasani, Optimal management of energy hubs and smart energy hubs – A review, Renew. Sustain. Energy Rev. 89 (2018) 33–50, http://dx.doi.org/10.1016/J.RSER.2018.02.035.

[4] P. Mancarella, MES (multi-energy systems): An overview of concepts and evaluation models, Energy 65 (2014) 1–17, http://dx.doi.org/10.1016/j.energy.2013.10.041.

[5] C. Forman, I.K. Muritala, R. Pardemann, B. Meyer, Estimating the global waste heat potential, Renew. Sustain. Energy Rev. 57 (2016) 1568–1579, http://dx.doi.org/10.1016/j.rser.2015.12.192.

[6] I. Al Asmi, R. Le Goff Latimier, H. Ben Ahmed, T. Esence, Impact of coupling thermal and electrical carriers on the optimal management of a multi-energy network, in: 2021 16th International Conference on Ecological Vehicles and Renewable Energies, EVER 2021, Institute of Electrical and Electronics Engineers Inc., 2021, http://dx.doi.org/10.1109/EVER52347.2021.9456613.

[7] V. Zinurov, M. Nikandrova, V. Kharkov, Assessment of thermal storage technologies in energy sector, in: 2020 Ural Smart Energy Conference (USEC), 2020, pp. 68–71, http://dx.doi.org/10.1109/USEC50097.2020.9281236.

[8] I. Al Asmi, K. Knobloch, R. Le Goff Latimier, T. Esence, K. Engelbrecht, H. Ben Ahmed, Thermocline thermal storage modeling towards its predictive optimal management, J. Energy Storage 52 (2022) 104979, http://dx.doi.org/10.1016/j.est.2022.104979.

[9] C.W. Forsberg, D.C. Stack, D. Curtis, G. Haratyk, N.A. Sepulveda, Converting excess low-price electricity into high-temperature stored heat for industry and high-value electricity production, Electr. J. 30 (6) (2017) 42–52, http://dx.doi.org/10.1016/j.tej.2017.06.009.

[10] Y. Lalau, I. Al Asmi, R. Olives, G. Dejean, A. Meffre, X. Py, Energy analysis and life cycle assessment of a thermal energy storage unit involving conventional or recycled storage materials and devoted to industrial waste heat valorisation, J. Clean. Prod. 330 (2022) 129950, http://dx.doi.org/10.1016/J.JCLEPRO.2021.129950.

[11] M. Cascetta, M. Petrollese, J. Oyekale, G. Cau, Thermocline vs. two-tank direct thermal storage system for concentrating solar power plants: A comparative techno-economic assessment, Int. J. Energy Res. 45 (2021) 17721–17737, http: //dx.doi.org/10.1002/ER.7005.

[12] F. Marongiu, S. Soprani, K. Engelbrecht, Modeling of high temperature thermal energy storage in rock beds – Experimental comparison and parametric study, Appl. Therm. Eng. 163 (2019) 114355, http://dx.doi.org/10.1016/j.applthermaleng.2019.114355.

[13] J.-F. Hoffmann, T. Fasquelle, V. Goetz, X. Py, Experimental and numerical investigation of a thermocline thermal energy storage tank, Appl. Therm. Eng. 114 (2017) 896–904, http://dx.doi.org/10.1016/j.applthermaleng.2016.12.053.

[14] I. Calderón-Vásquez, E. Cortés, J. García, V. Segovia, A. Caroca, C. Sarmiento, R. Barraza, J.M. Cardemil, Review on modeling approaches for packed-bed thermal storage systems, Renew. Sustain. Energy Rev. 143 (2021) http://dx.doi.org/10.1016/j.rser.2021.110902.

[15] A.C. Celador, M. Odriozola, J.M. Sala, Implications of the modelling of stratified hot water storage tanks in the simulation of CHP plants, Energy Convers. Manage. 52 (2011) 3018–3026, http://dx.doi.org/10.1016/j.enconman.2011.04.015.

[16] J.-F. Hoffmann, T. Fasquelle, V. Goetz, X. Py, A thermocline thermal energy storage system with filler materials for concentrated solar power plants: Experimental data and numerical model sensitivity to different experimental tank scales, Appl. Therm. Eng. 100 (2016) 753–761, http://dx.doi.org/10.1016/j.applthermaleng.2016.01.110.

[17] A. Touzo, R. Olives, G. Dejean, D. Pham Minh, M. El Hafi, J.-F. Hoffmann, X. Py, Experimental and numerical analysis of a packed-bed thermal energy storage system designed to recover high temperature waste heat: an industrial scale up, J. Energy Storage 32 (2020) 101894, http://dx.doi.org/10.1016/j.est.2020.101894.

[18] T. Esence, Étude et modélisation des systèmes de stockage thermique de type régénératif solide/fluide (Ph.D. thesis), Université Grenoble Alpes, 2017, URL: https://tel.archives-ouvertes.fr/tel-01714439.

[19] A. Bonanos, E. Votyakov, Analysis of thermocline thermal energy storage systems with generic initial condition algebraic model, Sol. Energy 213 (2021) 154–162, http://dx.doi.org/10.1016/j.solener.2020.11.011.

[20] E. Votyakov, A. Bonanos, A perturbation model for stratified thermal energy storage tanks, Int. J. Heat Mass Transfer 75 (2014) 218–223, http://dx.doi.org/10.1016/J.IJHEATMASSTRANSFER.2014.03.071.

[21] E.V. Votyakov, A.M. Bonanos, Algebraic model for thermocline thermal storage tank with filler material, Sol. Energy 122 (2015) 1154–1157, http://dx.doi.org/10.1016/J.SOLENER.2015.10.047.

[22] S.J. Cox, D. Kim, H. Cho, P. Mago, Real time optimal control of district cooling system with thermal energy storage using neural networks, Appl. Energy 238 (2019) 466–480, http://dx.doi.org/10.1016/j.apenergy.2019.01.093.

[23] J.B. Jørgensen, L.E. Sokoler, L. Standardi, R. Halvgaard, T.G. Hovgaard, G. Frison, N.K. Poulsen, H. Madsen, Economic MPC for a linear stochastic system of energy units, in: 2016 European Control Conference, ECC 2016, 2017, pp. 903–909, http://dx.doi.org/10.1109/ECC.2016.7810404.

[24] F. Verrilli, S. Srinivasan, G. Gambino, M. Canelli, M. Himanka, C.D. Vecchio, M. Sasso, L. Glielmo, Model predictive control-based optimal operations of district heating system with thermal energy storage and flexible loads, IEEE Trans. Autom. Sci. Eng. 14 (2017) 547–557, http://dx.doi.org/10.1109/TASE.2016.2618948.

[25] M. Leśko, W. Bujalski, K. Futyma, Operational optimization in district heating systems with the use of thermal energy storage, Energy 165 (2018) 902–915, http://dx.doi.org/10.1016/j.energy.2018.09.141.

[26] G. Limpens, S. Moret, H. Jeanmart, F. Maréchal, EnergyScope TD: A novel open-source model for regional energy systems, Appl. Energy 255 (2019) 113729, http://dx.doi.org/10.1016/j.apenergy.2019.113729.

[27] P. Gabrielli, M. Gazzani, E. Martelli, M. Mazzotti, Optimal design of multi-energy systems with seasonal storage, Appl. Energy 219 (2018) 408–424, http://dx.doi.org/10.1016/j.apenergy.2017.07.142.

[28] J. Cao, B. Yang, S. Zhu, C. Chen, X. Guan, Distributionally robust heat-and-electricity pricing for energy hub with uncertain demands, Electr. Power Syst. Res. 211 (2022) 108333, http://dx.doi.org/10.1016/j.epsr.2022.108333.

[29] R. Le Goff Latimier, T. Kovaltchouk, H. Ben Ahmed, B. Multon, Preliminary sizing of a collaborative system: Photovoltaic power plant and electric vehicle fleet, in: 2014 Ninth International Conference on Ecological Vehicles and Renewable Energies, EVER, 2014, pp. 1–9, http://dx.doi.org/10.1109/EVER.2014.6844110.

[30] R. Le Goff Latimier, B. Multon, H. Ben Ahmed, M. Acquitter, Cooptimisation de l'engagement de production et de la capacite de stockage associeea une ferme photovoltaique, prenant en compte le vieillissement de la batterie, in: Symposium de Génie Electrique SGE2014. ENS Cachan France, 2014.

[31] D.M. Rosewater, D.A. Copp, T.A. Nguyen, R.H. Byrne, S. Santoso, Battery energy storage models for optimal control, IEEE Access 7 (2019) 178357–178391, http://dx.doi.org/10.1109/ACCESS.2019.2957698.

[32] O. Ruhnau, L. Hirth, A. Praktiknjo, Time series of heat demand and heat pump efficiency for energy system modeling, Sci. Data 6 (2019) http://dx.doi.org/10.1038/s41597-019-0199-y.

[33] D. Ziyati, A. Dollet, G. Flamant, Y. Volut, E. Guillot, A. Vossier, A multiphysics model of large-scale compact PV–CSP hybrid plants, Appl. Energy 288 (2021) http://dx.doi.org/10.1016/j.apenergy.2021.116644.

[34] JRC Photovoltaic Geographical Information System (PVGIS) - European Commission, URL: https://re.jrc.ec.europa.eu/pvg_tools/en/.

[35] J.-F. Hoffmann, Stockage thermique pour centrale solaire thermodynamique à concentration mettant en oeuvre des matériaux céramiques naturels ou recyclés, Université de Perpignan, 2015, modele, URL: https://tel.archives-ouvertes.fr/tel-01284834.

[36] N. Wakao, T. Funazkri, Effect of fluid dispersion coefficients on particle-to-fluid mass transfer coefficients in packed beds: Correlation of sherwood numbers, Chem. Eng. Sci. 33 (10) (1978) 1375–1384, http://dx.doi.org/10.1016/0009-2509(78)85120-3, URL: https://www.sciencedirect.com/science/article/pii/0009250978851203.

[37] J. Coutier, E. Farber, Two applications of a numerical approach of heat transfer process within rock beds, Sol. Energy 29 (6) (1982) 451–462, http://dx.doi.org/10.1016/0038-092X(82)90053-6, URL: https://www.sciencedirect.com/science/article/pii/0038092X82900536.

[38] P. Virtanen, R. Gommers, T.E. Oliphant, M. Haberland, T. Reddy, D. Cournapeau, E. Burovski, P. Peterson, W. Weckesser, J. Bright, S.J. van der Walt, M. Brett, J. Wilson, K.J. Millman, N. Mayorov, A.R.J. Nelson, E. Jones, R. Kern, E. Larson, C.J. Carey, İ. Polat, Y. Feng, E.W. Moore, J. VanderPlas, D. Laxalde, J. Perktold, R. Cimrman, I. Henriksen, E.A. Quintero, C.R. Harris, A.M. Archibald, A.H. Ribeiro, F. Pedregosa, P. van Mulbregt, SciPy 1.0 Contributors, SciPy 1.0: Fundamental algorithms for scientific computing in Python, Nature Methods 17 (2020) 261–272, http://dx.doi.org/10.1038/s41592-019-0686-2.